

Active neuro-adaptive vibration suppression of a smart beam

Onur Akin^{1a} and Melin Şahin^{*2}

¹Aerospace Engineer, Department of Aerospace Engineering,
Middle East Technical University, Ankara, Turkey

²Department of Aerospace Engineering, Middle East Technical University, Ankara, Turkey

(Received October 5, 2016, Revised November 20, 2017, Accepted November 29, 2017)

Abstract. In this research, an active vibration suppression of a smart beam having piezoelectric sensor and actuators is investigated by designing separate controllers comprising a linear quadratic regulator and a neural network. Firstly, design of a smart beam which consists of a cantilever aluminum beam with surface bonded piezoelectric patches and a designed mechanism having a micro servomotor with a mass attached arm for obtaining variations in the frequency response function are presented. Secondly, the frequency response functions of the smart beam are investigated experimentally by using different piezoelectric patch combinations and the analytical models of the smart beam around its first resonance frequency region for various servomotor arm angle configurations are obtained. Then, a linear quadratic regulator controller is designed and used to simulate the suppression of free and forced vibrations which are performed both in time and frequency domain. In parallel to simulations, experiments are conducted to observe the closed loop behavior of the smart beam and the results are compared as well. Finally, active vibration suppression of the smart beam is investigated by using a linear controller with a neural network based adaptive element which is designed for the purpose of overcoming the undesired consequences due to variations in the real system.

Keywords: active vibration suppression; system identification; piezoelectricity; linear quadratic regulator; artificial neural network; performance comparison

1. Introduction

Suppression of undesirable vibrations is important because these vibrations can cause flutter, noise, structural failure, damage of equipment and even damage to human body. Suppression of vibrations are widely used in many applications such as in cars (Belgacem *et al.* 2012), hard disc drives (Yamada *et al.* 2007), telescopes (Schonhoff *et al.* 2000), railway vehicles (Foo and Goodall 2000), marine applications (Daley *et al.* 2004). Nowadays, being more lightweight, flexible and stiffer has the key importance in design of aerospace structures. But, these criteria lead unwanted oscillatory behavior in case of exposing dynamic loads and this affects the performance and the service life of the structure in an adverse way. Other negative effects that occur due to vibration of the aerospace structures are pollution created by the propulsion systems, low fuel efficiency because of increasing drag, less accuracy in satellite applications, unwanted effects on cabin crew and hardware of the aerospace vehicles.

In order to suppress vibrations of a structure, either passive or active techniques are used. Passive technique generally uses dampers, masses and springs in order to reduce the structural noise and/or vibrations (Mead 1998). But, usage of a passive technique is inefficient below

200 Hz and it increases weight of the structure which is an undesirable solution for the light weight aerospace structures (Ciminello *et al.* 2008). Therefore active techniques have been widely investigated and applied by the engineers. An active structure can sense external disturbances through sensors via transforming mechanical energy to electrical energy and it also has actuators to be excited for obtaining desirable behavior of the structure by transforming electrical energy into mechanical one.

An active vibration control has been used as a solution for vibration problems of aerospace structures for decades. Using piezoelectric materials as smart materials to suppress the vibration of a structure is an effective approach. For active vibration of structures, various control strategies have been developed. The research on active vibration suppression of structures was started using piezoelectric materials as sensors and actuators by Bailey and Hubbard (1985). They performed an experiment of the active vibration control on a cantilever beam using constant-gain and constant-amplitude controllers. Crawley and Luis (1987) presented a study about interaction between bonded piezoelectric elements and the substructure. They made tests on the first mode of the cantilever beam with distributed piezoelectric elements with three different test specimens. Fanson and Caughey (1990) implemented a positive position feedback (PPF) controller to control the first six bending modes of a cantilever beam by using piezoelectric materials for actuators and sensors. In addition to PPF control, Song *et al.* (2000) implemented strain rate feedback (SRF) control and their combinations. Manning, Plummer and Levesley (2000) designed a controller using

*Corresponding author, Ph.D., Assoc. Prof. Dr.

E-mail: msahin@metu.edu.tr

^aMSc.

E-mail: oakin.ae@gmail.com

pole placement to achieve a desired closed loop response and compared it with the velocity feedback controller. Caliskan (2002) developed PID and H_∞ controller to suppress the vibration of a cantilever beam and a fin successfully. Singh *et al.* (2003) implemented a controllers based on a method which is an extension of modified independent space control and compared it with the existing methods of independent modal space control (IMSC) and modified independent modal space control (MIMSC). Sahin *et al.* (2008) presented studies with H_∞ and μ -synthesis controllers which are intended to be used in the suppression of free and forced vibrations of the smart structures. In addition to these a sliding mode control (SMC) is also conducted (Itik *et al.* 2005). Vasques and Rodrigues (2006) implemented optimal control strategies, linear quadratic regulator (LQR), linear quadratic Gaussian (LQG) and compared them with the classical control strategies having constant gain and amplitude velocity feedback. There are studies which also include novel control algorithms used in vibration suppression field as genetic algorithm (Darus and Tokhi 2007), fuzzy logic (Wenzhong *et al.* 2004), and neural network (Kawabe *et al.* 2006).

In order to control the structure for decided performance criteria, a good analytical model of a smart structure is required but it may change due to various structural changes in structures (i.e., crack, boundary condition, variations in mass and stiffness properties, etc.). In order to make the controller robust, these variations that can occur in the structure are needed to be taken into consideration. In this research, analytical models of the smart structure are obtained experimentally for different configurations of the mass attached arm and a controller is designed for only one configuration. Effect of the plant variation to the closed loop behaviour is investigated and an adaptive element is added to overcome the undesired consequences due to variations in the system.

2. Design of the smart beam and experimental setup

A beam made of aluminium is used as the passive structure of the smart beam. The aluminum beam has dimensions of 35 cm x 3 cm with a thickness of 2 mm. At one end, the beam is clamped from 5 cm which makes the length of the vibrating part of the beam 30 cm. Sensor Technology BM500 (PZT - Lead Zirconate Titanate) is used as the piezoelectric patch. It has dimensions of 25.37 mm x 25.38 mm with a thickness of 0.57 mm. The dimensions of the clamped cantilever beam with bonded piezoelectric patches are shown in Fig. 1. Four piezoelectric patches are bonded on the beam. Two of them are on the front surface, the other two are on the back surface with the same distances from the fixed boundary. The piezoelectric patches are labelled as follows; piezo actuators (named and numbered as A1 & A2), a sensor piezo (named as S), a disturbance piezo (named as D). On the front surface; the piezoelectric patch on the root side is (A1), the other one is (S) and on the back surface; the piezoelectric patch on the root side is (A2) and the other one is (D) as shown in Fig. 2.

For bimorph configuration of the actuators, the cables

which are soldered on (A1) and (A2) are connected with opposite polarization (-'ve of A1 with +'ve of A2, +'ve of A1 with -'ve of A2) so that an applied voltage causes one of the piezoelectric patch to expand and the other to contract by providing a bimorph piezoelectric effect.

Mass variation is also considered in order to demonstrate a variation in the frequency response functions (FRF). By considering the maximum travel of the servomotor and the different arm lengths, the servomotor and a lumped mass are attached on different locations on the simple finite element model of the beam. After that, the first out-of-plane bending frequencies are obtained and listed by solving the finite element models. Therefore, location of the servomotor, arm length and lumped mass are decided to create at least 1 Hz difference in the first natural frequencies between the maximum clockwise and counterclockwise angles of the arm. The mass attached to the tip of the arm is chosen as 10 gr. The servomotor torque at 4.8 V is 0.176 Nm [21] and it is calculated that this value is much greater than the possible maximum torque created by the arm and the tip mass. For the control of the servomotor, an Arduino which is a physical computing platform based on simple microcontroller board is used to generate PWM (pulse width modification) signal. Five different configurations of the arm are considered. The midpoint of the servomotor where the arm is perpendicular to the beam is considered as 0°. Fig. 3 shows the different configurations of the arm and the labels as Case 1 (+64°), Case 2 (+32°), Case 3 (0°), Case 4 (-32°), Case 5 (-64°).

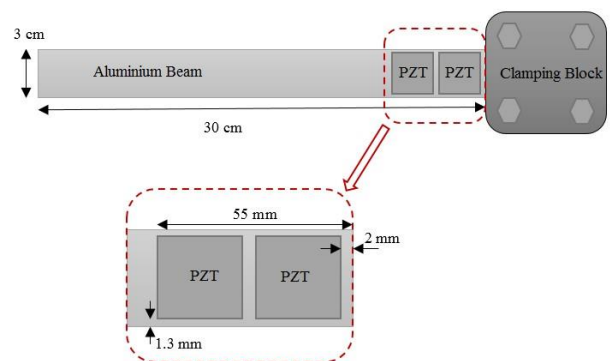


Fig. 1 Dimensions of the cantilever beam with piezoelectric patches

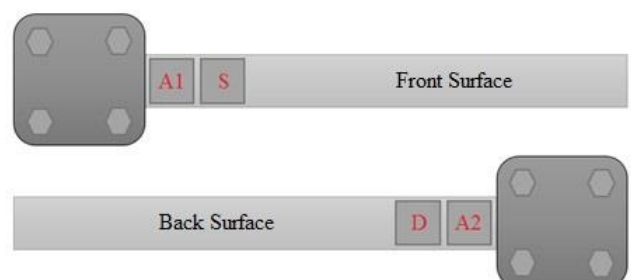


Fig. 2 Labels of the piezoelectric patches

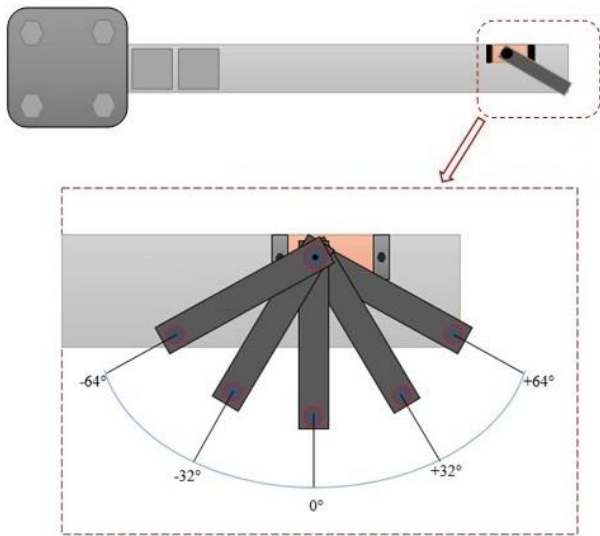


Fig. 3 Mass variation mechanism

Experimental setup consists of the smart beam (Fig. 4), a data acquisition system, an amplification system, and a sensor system. The data acquisition system includes a host pc and a target machine which are connected to each other.

The target machine is “Speedgoat Education Real-Time Target Machine” (2016) which is high-performance real-time simulation and testing platform. Since piezoelectric materials need high voltage for effective usage in active vibration control field. In this experimental setup, one high-voltage amplifier (Sensor Technology SA10, 2017) is installed to use both for disturbance and bimorph actuator signals as the SA10 high-voltage amplifier can be used as two individual amplifiers. To monitor the voltage of the piezoelectric patch (S) successfully, inverting voltage amplifier is used as piezoelectric materials generally have high impedance at low frequencies (Aridogan 2010). In addition, the voltage that the sensor piezoelectric patch (S) creates, is higher than the input voltage range of the data acquisition system. To get the voltage in the range of the input (i.e., ± 10 V), a voltage amplifier circuit is designed and the whole experimental setup is described schematically in Fig. 5.



Fig. 4 Smart beam

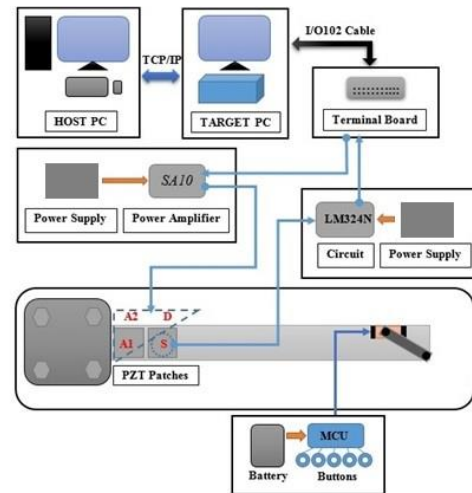


Fig. 5 Experimental setup

3. System identification of the smart beam

The smart beam is excited by the actuator piezoelectric patches (A1 & A2) for different servomotor arm angle configurations. The excitation signal is a swept-frequency cosine signal. In order to get the FRF of the smart beam for a specific servomotor arm configuration, an excitation signal is applied to the system and the response signal of the system is recorded by the xPC Target Machine for all cases in 1-100 Hz range. By analyzing the time domain data in MATLAB, experimental FRFs of (A1 & A2) – (S) PZT configuration for all arm angles are obtained. Fig. 6 shows the variation of the experimentally obtained frequency response functions of (A1&A2)-(S) PZT configuration of the smart beam. The frequency response functions are plotted in the range of 5 Hz - 40 Hz.

The experimental frequency response functions are converted to analytical models to be used as plants in designing controllers for vibration suppression of the smart beam. Transfer functions of the smart beam with different servomotor arm angle configurations are estimated in the range of 5 Hz - 30 Hz which includes the first resonance frequency region.

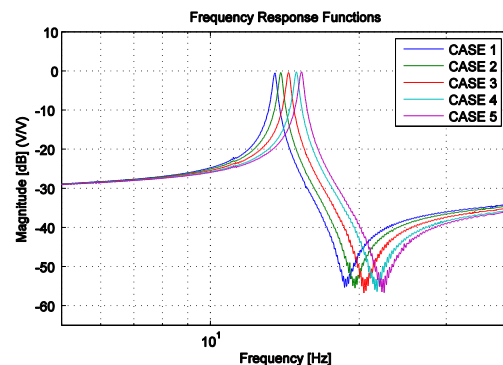


Fig. 6 Frequency response functions of (A1&A2)-(S) PZT configuration (All Cases)

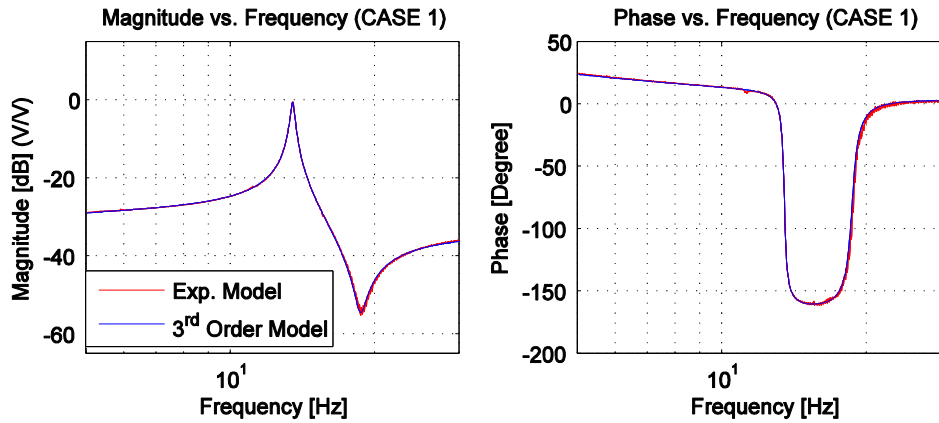


Fig. 7 Frequency response of experimental and 3rd order analytical model

Table 1 The first resonance frequencies and corresponding magnitudes of (A1&A2)-(S) PZT configuration of the smart beam for different arm angle cases

Arm Angle Cases	Resonance Frequency [Hz]	Magnitude at the Resonance Frequency [dB]
Case 1: +64°	13.50	-0.5858
Case 2: +32°	13.85	-0.6588
Case 3: 0°	14.38	-0.3312
Case 4: -32°	14.92	-0.2494
Case 5: -64°	15.30	-0.2300

To get accurate models, orders of the estimated transfer functions has to be high yet not computationally expensive. For finding the minimum necessary order, one of the arm angle configurations (+64° servomotor arm angle, Case 1) is chosen and different model orders (i.e., 1st, 2nd, 3rd, and 4th) are tested. It is found that 3rd order is enough for representing the FRF which covers the first resonance frequency of the smart beam (Fig. 7).

For all servomotor arm angle configurations, 3rd order estimated continuous transfer functions are obtained. The first resonance frequencies and the corresponding magnitudes are shown in Table 1. As it can be seen from Table 1, the first resonance frequency of the smart beam increases as the mass attached arm moves towards to the root of the beam (From +64° to -64° arm angle). The estimated transfer functions for each servomotor arm angle are listed in the Table 2.

4. Active vibration suppression of the smart beam by using Linear Quadratic Regulator (LQR) method

Linear time-invariant state-space model of the smart beam is represented as

$$\dot{x} = Ax(t) + Bu(t) \quad (1)$$

$$y = Cx(t) + Du(t) \quad (2)$$

y are not vectors, in fact, they are scalars. The output y is used to simulate data measured from the piezoelectric patch sensor (S) and the input u is used to simulate signal transmission to the piezoelectric patches (A1&A2) through the amplifier.

The Linear Quadratic Regulator (LQR) is an optimal controller that uses all the states of the plant and creates a feedback signal as a function of the states.

One of the advantages of the LQR controller is that stability is guaranteed if all the states in the system are available and if the model resembles the dynamic system well. Before designing the controller, controllability of the system has to be verified. As the system is found as controllable, all the states can be driven. The vector of state-feedback control gains represented as K and the control input of the system is shown as in Eq. (3).

$$u(t) = -Kx(t) \quad (3)$$

Performance index of the LQR controller is shown in Eq. (4) where $u(t)$ is input vector and $x(t)$ is state vector of the system in time domain.

$$J = \frac{1}{2} \int_0^{\infty} [x^T(t)Qx(t) + u^T(t)Ru(t)]dt \quad (4)$$

where Q is a positive-semidefinite state variable and R is a positive-definite input variable weighting matrices. In order to achieve an optimal control, the performance index J has to be minimal. After analyzing the performance index equation, the optimal control input which minimizes the performance index is found as in Eq. (5).

$$u = -R^{-1}B^T Px \quad (5)$$

So, full state-feedback gain vector K is found as in Eq. (6).

$$K = -R^{-1}B^T P \quad (6)$$

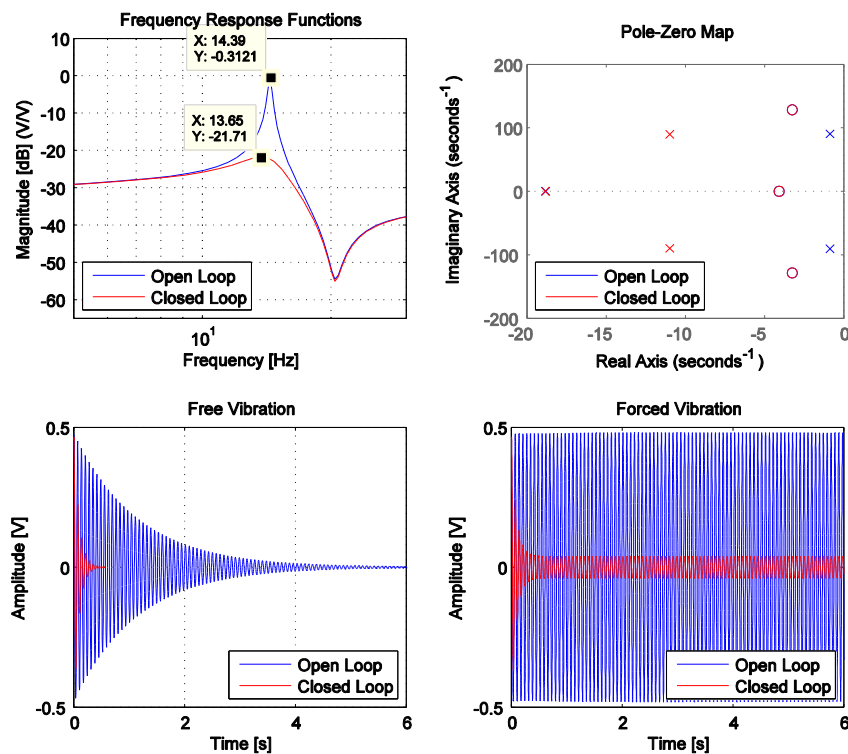
Here, R is a weighting matrix of the LQR controller and B is the control matrix of the plant. The parameter P is calculated by using algebraic Riccati equation which can be seen in Eq. (7).

Table 2 Analytical models of the (A1&A2)-(S) PZT configuration of the smart beam for different arm angle cases

Arm Angle Cases	Continuous-Time Transfer Functions
Case 1: +64°	$G_1(s) = \frac{0.01996 s^3 + 0.2001 s^2 + 275.7 s + 1291}{s^3 + 21.11 s^2 + 7228 s + 1.403e05}$
Case 2: +32°	$G_2(s) = \frac{0.01943 s^3 + 0.1975 s^2 + 290.1 s + 1231}{s^3 + 20.64 s^2 + 7641 s + 1.443e05}$
Case 3: 0°	$G_3(s) = \frac{0.01879 s^3 + 0.1993 s^2 + 310.7 s + 1269}{s^3 + 20.58 s^2 + 8214 s + 1.539e05}$
Case 4: -32°	$G_4(s) = \frac{0.01816 s^3 + 0.2039 s^2 + 333.4 s + 1326}{s^3 + 20.54 s^2 + 8838 s + 1.644e05}$
Case 5: -64°	$G_5(s) = \frac{0.01784 s^3 + 0.2058 s^2 + 349.1 s + 1380}{s^3 + 20.63 s^2 + 9260 s + 1.725e05}$

Table 3 Results of the LQR Controller Simulations

Parameters	Gain [dB]	Controller Output[V] (Maximum Absolute)	Settling Time [s]	Forced Vibration Suppression
$\alpha=1, \beta=1$	-1.17	0.14	4.5	12%
$\alpha=1, \beta=0.1$	-6.11	0.96	2.57	50%
$\alpha=1, \beta=0.01$	-14.97	3.93	0.95	82%
$\alpha=1, \beta=0.002$	-21.40	8.40	0.42	92%
$\alpha=1, \beta=0.001$	-23.92	10.80	0.30	94%

Fig. 8 Simulation results for $\beta=0.002$

$$A^T P + PA - BPR^{-1}B^T P + Q = 0 \quad (7)$$

Thus, to achieve a desired response of the dynamic system, the required gain vector K can be calculated by tuning Q and R parameters. Q is a matrix and R is a scalar value as there is only one control input to the system. The matrix Q (Eq. (8)) is chosen as a 3 by 3 identity matrix multiplied by a parameter α . For the scalar R value (Eq. (9)), symbol β is used. In this study, α is chosen as 1 and β is used as a variable and is changed to obtain maximum vibration suppression performance.

$$Q = \alpha \times \begin{bmatrix} 1 & 0 & 0 \\ 0 & 1 & 0 \\ 0 & 0 & 1 \end{bmatrix} \quad (8)$$

$$R = \beta \quad (9)$$

The full state feedback gain vector “ K ” is obtained by using Matlab. After obtaining the “ K ” vector, frequency response functions, pole-zero maps, free vibration responses and forced vibration responses are plotted for different β values. Without the controller, the settling time for the initial condition x_0 is approximately 5.2 seconds with an error band of ± 0.005 V. The variable β is decreased until the maximum voltage of the controller output is passed the maximum allowed input voltage of the system (i.e., 9 V) and the performance of the controllers are observed. From the Table 3, it can be seen that the controller having maximum performance for the initial condition is obtained for $\alpha=1$, $\beta=0.002$ values. Fig. 8 shows the frequency response functions, pole-zero map, free and forced vibration responses of the open and closed systems by using the parameters. This, so called the best performance controller decreased the settling time of the system from 5.2 seconds to 0.42 seconds for the given initial condition. It also decreased the forced vibration amplitude by approximately 92 %.

In experimental studies, in order to control the vibrations of the smart beam via LQR controller, all the states have to be measurable. But, only the output ‘ y ’ which is measured from the sensor piezoelectric patch (S) of the smart beam is available. Observability of the system should be checked and hence, one way of dealing with this problem is designing an observer for the states of the dynamic system. In this study, instead of designing an observer, desired closed loop behavior of the system is obtained by using MATLAB and Simulink platforms and after obtaining the desired closed loop transfer function of the system and by using the transfer function of the plant, a controller transfer function is calculated to be used in an output feedback control system (Fig. 9). Reference is set to 0 which is a desired output value for vibration suppression.

The desired closed loop transfer function of the system is given in Eq. (10) and also from Eq. (9), the below (Eq. (11)) is obtained as

$$\frac{Y(s)}{D(s)} = G_{closed\ loop}(s) \quad (10)$$

$$Y(s) = (-Y(s) \times G_{controller}(s) + D(s)) \times G_{plant}(s) \quad (11)$$

By using Eq. (11), the following (Eq. (12)) closed loop transfer function of the system can be calculated. Thus, the controller transfer function can be written in terms of the transfer function of the plant and the closed loop transfer function of the system as in the Eq. (13).

$$\frac{Y(s)}{D(s)} = \frac{G_{plant}(s)}{(G_{plant}(s) \times G_{controller}(s)) + 1} \quad (12)$$

The closed loop transfer function of the smart beam with 0° servomotor arm angle configuration is calculated by using the Eq. (14) where $\alpha=1$, $\beta=0.002$.

$$G_{controller}(s) = \frac{G_{plant}(s) - G_{closed\ loop}(s)}{G_{closed\ loop}(s) \times G_{plant}(s)} \quad (13)$$

$$G_{closed\ loop}(s) = \frac{0.01879 s^3 + 0.1993 s^2 + 310.8 s + 1269}{s^3 + 40.8 s^2 + 8584 s + 1.539e05} \quad (14)$$

Transfer function of the plant model is known and therefore the transfer function used for a controller in the experimental studies can be calculated by using the Eq. (15).

$$G_{controller}(s) = \frac{1076 s^2 + 1.972e04 s + 0.08642}{s^3 + 10.6 s^2 + 1.653e04 s + 6.752e04} \quad (15)$$

Without giving any disturbance and control signal to the system, the maximum noise level is measured as 0.0120 V and the DC offset of the sensor is obtained as -0.0175 V. This value is subtracted from the input module Simulink block of the xPC Target Machine. Analysis of the free vibration of the smart beam is performed by giving a displacement to the tip of the smart beam which makes the initial measured sensor value approximately ± 0.48 V. In the first bending mode, displacement at the tip of the smart beam corresponds to the maximum curvature at the root of the smart beam. The displacement range at the tip of the smart beam is measured as approximately 1 mm when the measured value from the analog input of the target machine is observed as ± 0.48 V. In Fig. 10, open and closed system time responses to the initial condition and the corresponding controller signal is shown. The comparison of the free vibration suppression simulation and experiment results of the smart beam to the given the initial condition is shown in Table 4. It is found that the experimental results are close to the results obtained by the simulations.

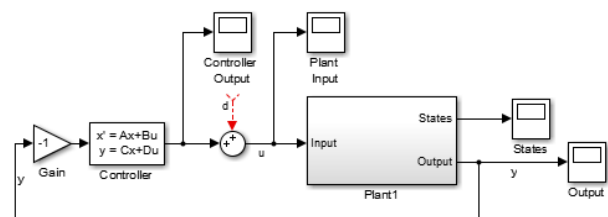


Fig 9 Output feedback control system simulink block diagram

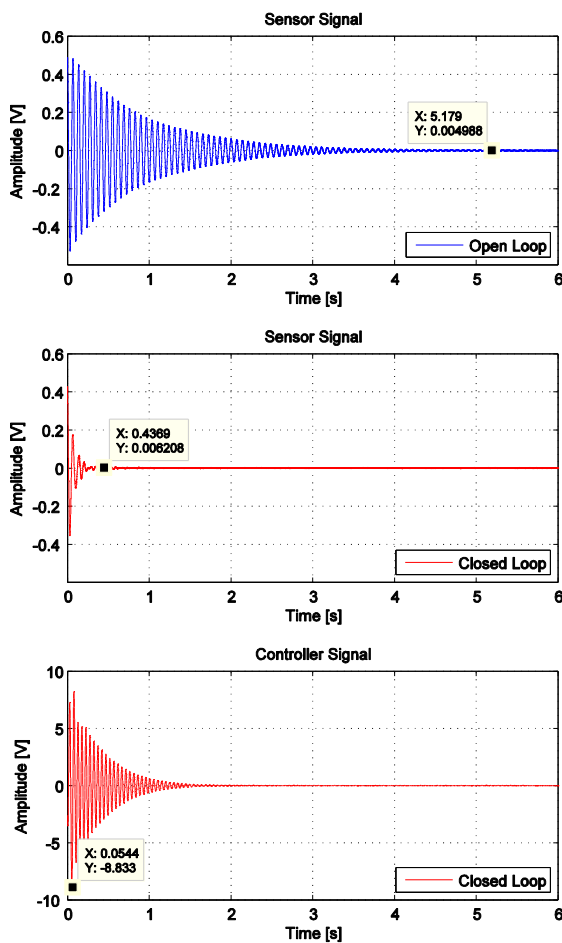


Fig 10 Plots of the free vibration suppression experiments

Analysis of the first resonance forced vibration suppression is performed by applying a sine wave at 14.38 Hz frequency to the disturbance piezoelectric patch (D) and applying a controller signal to the actuator piezoelectric patches (A1&A2). Forced vibration simulations were made for the vibrating beam when the sensor amplitude shows ± 0.48 V. This experiment lasts 30 seconds. First, a sine wave at the smart beam's resonance frequency is applied 10 seconds (i.e., Open loop system). After that the controller is applied to the system for again 10 seconds (i.e., Closed loop system) and then, the controller is removed to let the smart beam vibrate at its first resonance frequency again (i.e., Open loop system). Fig. 11 shows the recorded sensor and controller signals of the first resonance forced vibration suppression experiment. The open and the closed loop response plots of the forced vibration experiments of the smart beam can also be seen in Fig. 12.

The forced vibration suppression performance of the controller is calculated as 89 % which is very close to the percentage value obtained by the simulations. Table 5 shows the comparison of the forced vibration suppression simulation and experiment results of the smart beam.

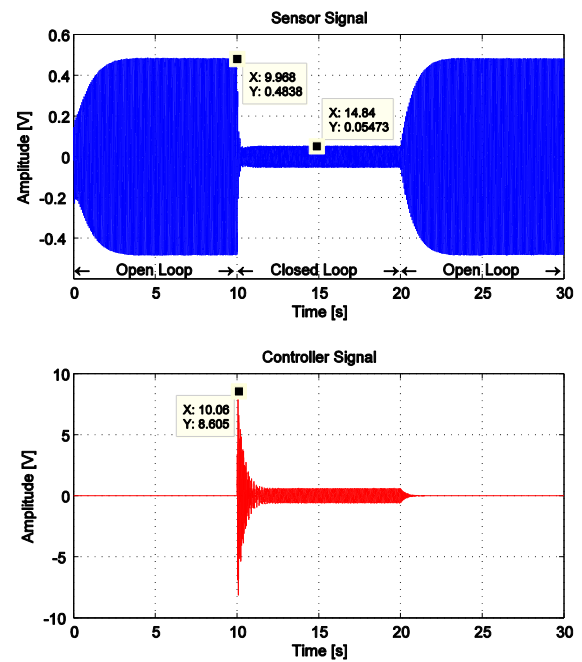


Fig 11 Plots of the forced vibration suppression experiment

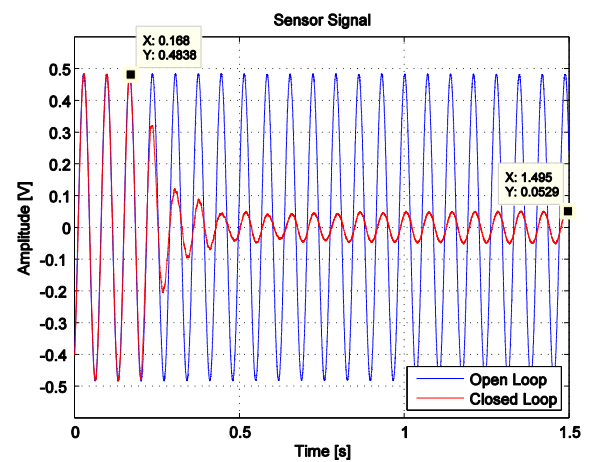


Fig 12 Open and closed loop plots of the forced vibration experiments

Experiments are performed in order to obtain the frequency response functions for both open and closed loop systems. The frequency response functions can be seen in Fig. 13. The obtained closed loop experimental results are observed to be in good agreement with the simulation results. Effect of the plant variation to the closed loop system is investigated by using the designed controller to the other configurations. The designed controller is used to control the vibrations of the smart beam for the Case 3 (0° arm angle configuration) successfully but if the controller is kept the same and the arm angle of the smart beam is changed to various configurations, the corresponding behavior of the closed loop system changes.

Table 4 Free vibration suppression simulation and experiment results

	Settling Time [s]		Controller Output [V] (Maximum Absolute)
	Open Loop	Closed Loop	
Simulation	5.20	0.42	8.40
Experiment	5.18	0.44	8.83

Table 5 Forced vibration suppression simulation and experiment results

	Suppression Performance (Percentage)	Controller Output [V] (Maximum Absolute)
Simulation	92%	8.40
Experiment	89%	8.60

It is observed that the controller and the plant combinations (i.e., For Case 1, Case 2, and Case 4) are stable except the Case 5 as shown in Fig. 14. The particular case has poles on the right half plane of the complex plane and these poles are corresponding to the frequency of 20.7 Hz making the system unstable.

It is observed that as servomotor arm moves to the tip of the smart beam, the forced vibration suppression performance decreases at the corresponding frequencies. On the contrary, the forced vibration suppression performance increases as the arm moves towards to the root of the smart beam. The dB levels are close to each other for all the cases. However, using the designed controller (i.e., the control designed for Case 3) to the plant in Case 5 making the closed loop system unstable which is a problem to be considered. For this particular case, an experiment is conducted to observe the unstable behavior of the closed loop system.

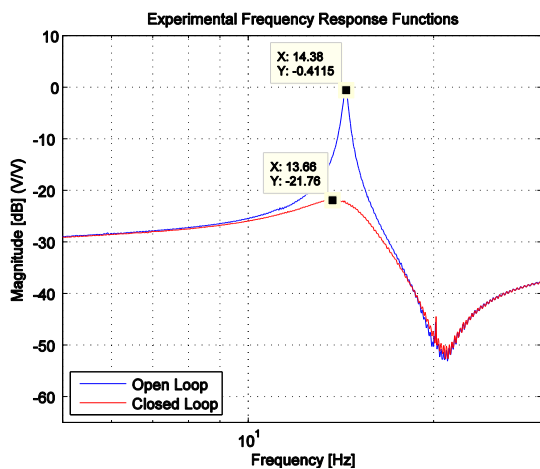


Fig 13 Experimental open and closed loop frequency response functions

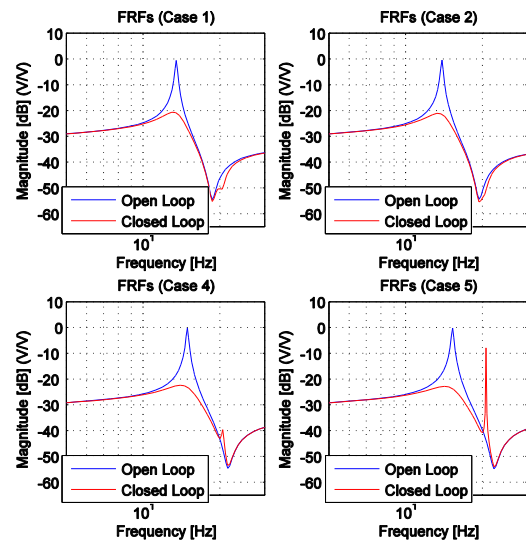


Fig 14 Frequency response functions for different closed loop systems

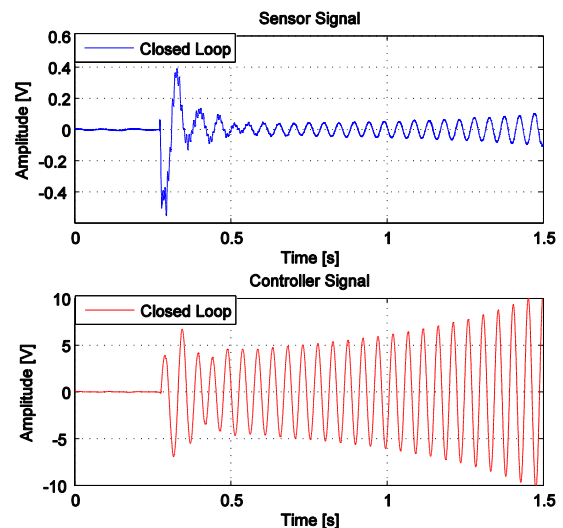


Fig 15 Experimental results for case 5 (-64° Arm Angle)

There is not a specific sine wave disturbance in this experiment but there is a disturbance which is externally applied in a short time at the tip of the smart beam. Then, the response of the smart beam is recorded as shown in the Fig. 15 and the divergent signal frequency is found as approximately 20.7 Hz as expected.

5. Active vibration suppression of the smart beam by adding a neural network based adaptive element

In this part, a neural network based adaptive element is designed and added to the system to overcome the problem occurs due to plant variation. By changing the parameters of

the LQR method, it is possible to design a controller that the closed loop system for Case 5 is not unstable but in this case, the performance of the suppression of the smart beam would be less. The aim of designing neural network based adaptive element to the system is to solve the instability problem without losing desired performance. A multilayer feedforward neural network with back propagation algorithm (Haykin 2005) is designed for the adaptive element. For the activation function, hyperbolic tangent sigmoid is used. The output voltage range between -1 to 1 is suitable for vibration control signals but to apply signal within the voltage range of the smart beam system, scaling factor is applied. There might be a case such as there is a signal source at a specific frequency or combination of frequencies applied to the structure which does not create much problem considering the amplitude of the vibration of the structure. In case of variation of the frequency response function of the structure like change in boundary condition, connections on the structure, mass, crack etc. one of the resonance frequencies of the structure may match with frequency content of the disturbance signal.

As it can be seen in Fig. 15, using the designed controller to the plant in Case 5 makes the closed loop system unstable. In order to observe this behavior, changing the configuration from Case 4 to 5 is chosen. It is considered that disturbance signal of the smart beam is the sine wave at a frequency of 15.30 Hz but the smart beam configuration is at the Case 4 (i.e., the resonance frequency of 14.92 Hz and servomotor arm angle of -32°). In this case, the smart beam vibrates at a low vibration level of -9.2 dB.

In case of a variation in the frequency response function of the smart beam which can be achieved by changing the servomotor arm angle (from Case 4 to Case 5), the smart beam's vibration amplitude starts to increase and reaches to the vibration level of -0.22 dB. Fig. 16 shows the frequency response functions of the smart beam at servomotor arm angles of -32° (Case 4) and -64° (Case 5).

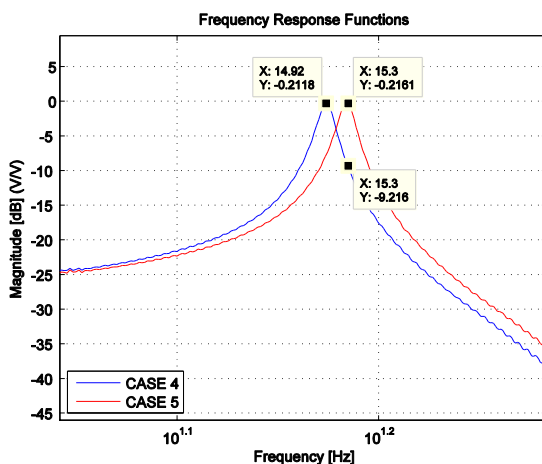


Fig 16 Frequency response functions of the smart beam for Case 4 and 5

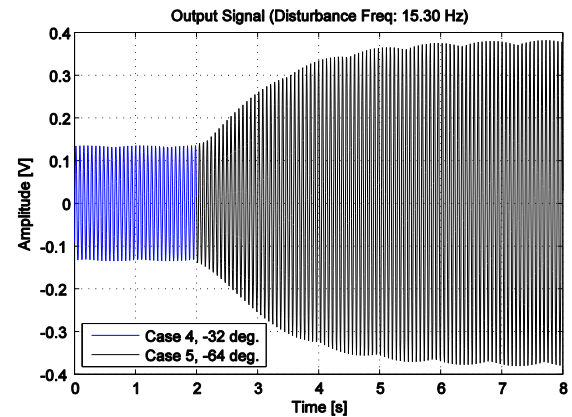


Fig 17 Simulation result of the plant variation

In order to simulate plant variation while the system is operating, a Simulink block namely “variable plant” is designed. It changes the matrices of the state-space form of the smart beam at an arm angle case to another arm angle case's matrices. The input signal of the plant is kept constant as 15.30 Hz which is the first resonance frequency of the plant in Case 5. Then, the servomotor arm angle is changed from -32° (i.e., Case 4) to -64° (i.e., Case 5) at a time of 2 seconds. The following figure (Fig. 17) presents the result of the variation in the frequency response function of the plant.

A neural network controller is desired to be used for suppression of the smart beam via handling the variations in the FRF of the smart beam. In Calise *et al.* (2001) and (2004), details of controlling of a flexible system method are described. This method is implemented to the vibration suppression study hence tracking purpose is not used so that the reference is chosen as a zero consideration on the offset of the sensor. The previously designed controller (i.e., LQR controller in section four) and a reference model (i.e., Case 3) are used in the adaptive controller design. The neural network works as an element to handle the difference between the reference model output and the real system output. This difference depends on the states of the reference model, the states of the real system and the input of the real system. However, states of the real system are not measurable. Only the output of the real system is measured from the piezoelectric sensor patch. As the system is observable, the states of the real system can be obtained by using previously obtained data of the input and the output of the real system. Thus, the inputs of the neural network are taken as the previous values of the output, the input of the real system and the states of the reference model. In order to simulate an active vibration suppression, random weights are chosen to train the neural network and simulations are restarted for several times with random weights until the desired error energy is obtained.

The weights obtained after a successful simulation are saved to be used for the further cases (i.e., variations in plant scenarios) as initial weights. It was presented that the system with -64° arm angle (i.e., Case 5) is unstable if the controller designed for the Case 3 is used. Firstly, a simulation is performed to observe the instability of the

system when the arm changes from Case 4 to Case 5. Then, a neural network based adaptive element is added to the block diagram and another simulation is performed. It is shown that the system with controller designed by using LQR method and the neural network together can suppress the vibrations without being affected by this plant variation. The arm angle is then changed intentionally at particular time (i.e., at 2 second) and the results of the simulations are shown in Fig. 18.

After the variation, the system only with the designed controller becomes unstable as expected. With the neural network based adaptive element, the system keeps the vibrations of the plant suppressed by making the system stable. The suppression performance at the first resonance frequency of the plant with Case 5 is obtained approximately as 88% which is very close to the result obtained from the simulations performed for the Case 3 in section four.

Free vibration suppressions of the plant without controller, with the previously designed controller only and with the neural network added controller for -64° servomotor arm angle (Case 5) are also performed. The initial states of the plant are obtained by using the same procedure presented in part 4 and used to simulate free vibration of the plant. Fig. 19 shows the results of the free vibration suppression simulations. Free vibration suppression of the plant without controller lasts for approximately 3.5 seconds. With the controller designed by using LQR method, the settling time is approximately found as 0.5 seconds but as the controller designed for the Case 3 is used for the Case 5, the system starts to vibrate at the frequency of the unstable pole which is at 20.7 Hz. Moreover, the neural network based adaptive element is added to the block diagram and as a result, the closed loop system is obtained as a stable system and the settling time is found as approximately 0.7 seconds.

Experimental studies are conducted to analyze the free and forced vibration suppression behaviors of the controller designed in section four (i.e., LQR Controller) and the controller with the neural network in case of arm angle variation from -32° (i.e., Case 4) to -64° (i.e., Case 5). Firstly, an experiment is conducted to observe the increase in vibration level of the beam after changing the servomotor arm from -32 to -64 . The disturbance signal's frequency is 15.30 Hz which is the resonance frequency of the plant in the arm configuration of Case 5. The servomotor arm angle is changed at a particular time (i.e., at 2 second) and the response of the smart beam to the FRF variation without the controller is plotted (Fig. 20).

Secondly, by adding the controller which is designed by LQR method to the block diagram, the behavior of the smart beam to the variation of the servomotor arm angle from -32° to the -64° is observed. Then, the neural network is added to the block diagram and an experiment is conducted again. The response of the smart beam is observed as stable and the vibration suppression performance of the system is found as 89% which is very close to the result obtained in the simulation studies. All these results are presented in Fig. 21.

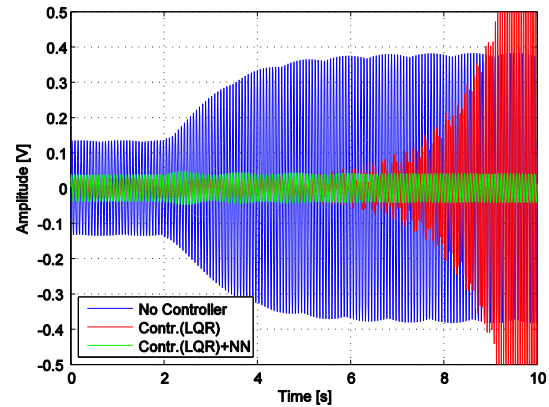


Fig 18 Results of forced vibration suppression simulations

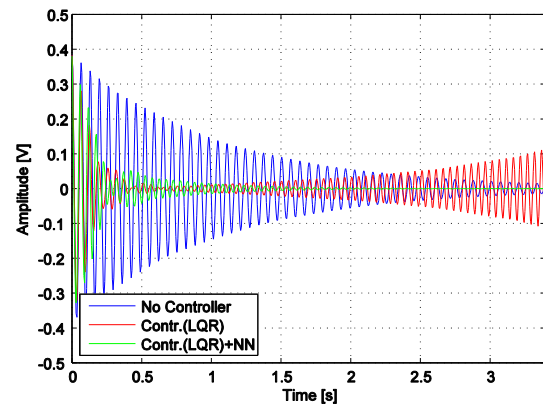


Fig 19 Results of free vibration suppression simulations

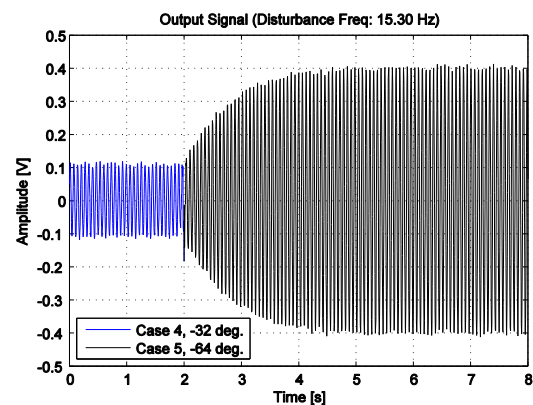


Fig 20 Experimental result of the plant variation

Moreover, free vibration responses of the smart beam without controller, with the controller designed by using LQR method and with the neural network based adaptive element added system are experimentally obtained and the results which are shown in Fig. 22 are in good agreement with the simulation results.

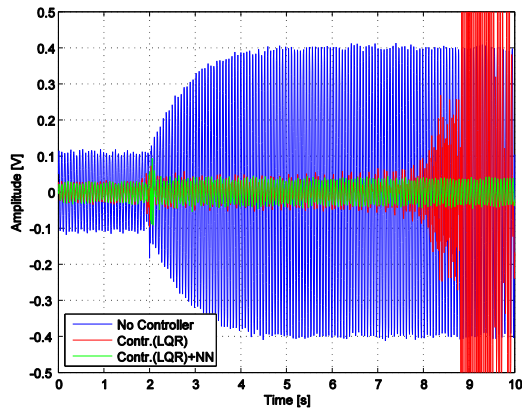


Fig 21 Results of the forced vibration suppression experiments

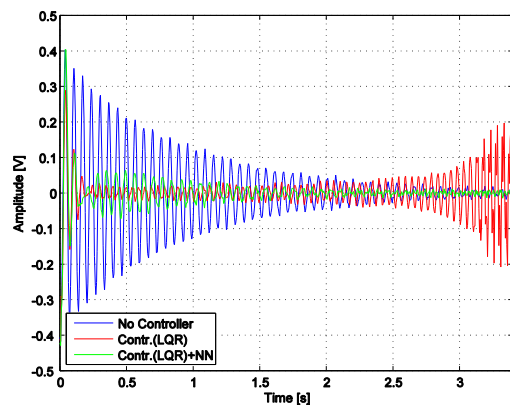


Fig 22 Results of the free vibration suppression experiments

6. Conclusions

This paper finally shows that sufficient vibration suppression levels are reached in the smart beam structure through linear quadratic regulator and an artificial neural network based control algorithms via piezoelectric sensor and actuators in the cases where there are some variations in the frequency response function of the structure around its first resonance frequency region.

Acknowledgments

The authors gratefully acknowledge the support provided by the Middle East Technical University under grant number BAP-03-13-2014-001 for the project titled "Active Vibration Suppression of Aerospace Structures with Piezoelectric Materials via Novel Adaptive Controllers".

References

Aridogan, M.U. (2010), "Performance evaluation of piezoelectric sensor/actuator on investigation of vibration characteristics and active vibration control of a smart beam", MSc. Dissertation,

- Middle East Technical University, Ankara.
- Bailey, T. and Hubbard, J.E. (1985), "Distributed piezoelectric-polymer active vibration control of a cantilever beam", *J. Guid. Control. Dynam.*, **8**(5), 605-611.
- Belgacem, W., Berry, A. and Masson, P. (2012), "Active vibration control on a quarter-car for cancellation of road noise disturbance", *J. Sound Vib.*, **331**(14), 3240-3254.
- Calise, A.J., Hovakimyan, N. and Idan, M. (2001), "Adaptive output feedback control of nonlinear systems using neural networks", *Automatica*, **37**(8), 1201-1211.
- Calise, A.J., Yang, B.J. and Craig, J.I. (2004), "Augmenting adaptive approach to control of flexible systems", *J. Guid. Control. Dynam.*, **27**(3), 387-396.
- Çalışkan, T. (2002), "Piezoelectric ceramics and their applications in smart aerospace structures", Ph.D. Dissertation, Middle East Technical University, Ankara.
- Ciminello, M., Calabro, A., Ameduri, S. and Concilio, A. (2008), "Synchronized switched shunt control technique applied on a cantilevered beam: Numerical and experimental investigations", *J. Intel. Mat. Syst. Str.*, **19**, 1089-1100.
- Crawley, E.F. and De Luis, J. (1987), "Use of piezoelectric actuators as elements of intelligent structures", *AIAA J.*, **25**(10),
- Daley, S., Johnson, F.A., Pearson, J.B. and Dixon, R. (2004), "Active vibration control for marine applications", *Control Eng. Pract.*, **12**(4), 465-474
- Darus, I.Z.M. and Tokhi, M.O. (2007), "Genetic algorithm active vibration control of flexible plate structures", *Proceedings of the 51st Annu. Meet. ISSS*, Tokyo, Japan.
- Fanson, J.L. and Caughey, T.K. (1990), "Positive position feedback control for large space structures", *AIAA J.*, **28**(4), 717-724.
- Foo, E. and Goodall, R.M. (2000), "Active suspension control of flexible-bodied railway vehicles using electro-hydraulic and electro-magnetic actuators", *Control Eng. Pract.*, **8**(5), 507-518.
- Haykin, S. (2008), *Neural Networks and Learning Machines*, 3rd Ed., Pearson Education, Hamilton, Ontario, Canada.
- http://www.savoxusa.com/Savox_SH0253_Micro_Digital_Servo_p/savsh0253.htm (accessed October 04, 2016).
- Itik, M., Salamci, M., Ulker, F.D. and Yaman, Y. (2005), "Active vibration suppression of a flexible beam via sliding mode and Hinf control", *Proceedings of the 44th IEEE Conf. Decis. Control. Eur. Control Conf.*, Seville, Spain.
- Kawabe, H., Tsukiyama, N. and Yoshida, K. (2006), "Active vibration damping based on neural network theory", *Mater. Sci. Eng. A.*, **442**(1-2), 547-550.
- Manning, W.J., Plummer, A.R. and Levesley, M.C. (2000), "Vibration control of a flexible beam with integrated actuators and sensors", *Smart Mater. Struct.*, **9**(6), 932-939.
- Mead, D.J. (1998), *Passive Vibration Control*, 1st Ed., Wiley, Chichester, New York, USA.
- Sahin, M., Karadal, F.M., Yaman, Y., Kircali, O.F., Nalbantoglu, V., Ulker, F.D. *et al.* (2008), "Smart structures and their applications on active vibration control: studies in the department of aerospace engineering, METU", *J. Electroceramics.*, **20**(3-4), 167-174.
- Savox SH-0253 Micro Digital Servo,
- Schonhoff, U., Klein, A. and Nordmann, R. (2000), "Attitude control of the airborne telescope SOFIA: mu-synthesis for a large scaled flexible structure", *Proceedings of the 39th IEEE Conf. Decis. Control (Cat. No.00CH37187)*, 3576-3581.
- Sensor Technology, <http://sensortechcanada.com/> (accessed October 04, 2016).
- Singh, S.P., Pruthi, H.S. and Agarwal, V.P. (2003), "Efficient modal control strategies for active control of vibrations", *J. Sound Vib.*, **262**(3), 563-575.
- Song, G., Schmidt, S.P. and Agrawal, B.N. (2000), "Active vibration suppression of a flexible structure using smart

- material and a modular control patch”, *Proc. Inst. Mech. Eng. Part G-Journal Aerosp. Eng.*, **214**, 217-229.
- Speedgoat Educational Real-Time Target Machine, <http://www.mathworks.com/hardware-support/xpc-target-turnkey.html> (accessed October 04, 2016).
- Vasques, C.M.A. and Rodrigues, J.D. (2006), “Active vibration control of smart piezoelectric beams: Comparison of classical and optimal feedback control strategies”, *Comput. Struct.*, **84**(22-23), 1402-1414.
- Wenzhong, Q., Jincui, S. and Yang, Q. (2004), “Active control of vibration using a fuzzy control method”, *J. Sound Vib.*, **275**(3-5), 917-930.
- Yamada, H., Sasaki, M. and Nam, Y. (2007), “Active vibration control of a micro-actuator for hard disk drives using self-sensing actuator”, *J. Intel. Mat. Syst. Str.*, **19**, 113-123.

CC